10.1109/ULTSYM.2015.0198

Improving Lateral Resolution in Ultrasonic Imaging by Utilizing Nulls in the Beam Pattern

Jonathan Reeg, *Student Member, IEEE*, Michael L. Oelze, *Senior Member, IEEE*

***Abstract*—Reduction of lateral sidelobes results in improved ultrasonic imaging. In general, apodization is used to lower sidelobes in exchange for increasing the width of the mainlobe and thus decreasing lateral resolution. Null Subtraction Imaging (NSI) is a technique that uses different on-receive apodizations on copies of the same image to to reduce sidelobe levels while also improving lateral resolution. In the NSI technique, several apodization functions are applied on receive. The first apodization weight is applied having a zero mean value when summed across the aperture. This places a null at the broadside of the receive pattern. The second apodization is the same as the first apodization except that a constant offset in weight is applied (non-zero mean). The third apodization is the transpose of the second. The images created with the different weighting schemes are then added to form a new image with improved sidelobe performance and dramatically better lateral resolution compared to conventional apodization. To evaluate the performance of this technique, experiments were performed with an ATS539 phantom containing wire targets to assess lateral resolution and cylinder targets to assess contrast. A 9L4 array was used in the measurements connected to an Ultrasonix RP system with a SonixDAQ. Plane waves were emitted from the array and ultrasound echoes were received by each array element. Image reconstruction involved using Delay and Sum beamforming with apodization. Images were constructed using NSI and compared with rectangular weighted apertures. In experiments, the lateral resolution was observed to improve by a factor of five or better when compared to rectangular apodization. Image quality was assessed by estimation of lateral resolution (-3-dB receive beamwidth), the mainlobe to sidelobe ratio (MSR) in dB and estimation of the contrast-to-noise ratio (CNR). At f/# = 1 focusing with NSI, the -6-dB beamwidth on receive as measured from a small wire target in the ATS phantom was 0.414λ. Sidelobes were observed to decrease at each f/# by an average of 17 dB with NSI compared to rectangular apodization. However, contrast of hyperechoic targets were lost when utilizing the NSI scheme.**

***Index Terms*—Ultrasound imaging, Apodization, Beamforming, Superresolution**

I. Introduction

In modern ultrasonic imaging, backscattered echo data are captured by transducers, typically in the form of an array of elements. These transducers send out pulses of ultrasound and then listen for echoes. In conventional B-mode imaging, the received signals composed from these echoes are beamformed, envelope detected, and then the collective signals are stacked together to create the image. On both transmission and reception, weights may be assigned to the elements of a transducer array to shape its radiation pattern. This weighting is called apodization.

Apodization of the transducer elements is analogous to windowing a time-domain signal. Choosing a window function that reduces the sidelobes while still maintaining an optimal mainlobe width is a classical problem in signal analysis. For most apodization schemes, reducing the sidelobes through apodization has the tradeoff of widening the mainlobe [1]. In 1946, Dolph developed a weighting method, or apodization, using Chebyshev polynomials for a linear array antenna that shaped its radiation pattern such that the minimum mainlobe width was achieved for a given maximum sidelobe level [2]. In 1982, t'Hoen did a study applying nine different apodization schemes to a linear ultrasound array and studying their effects on the image quality, finding that four of these schemes (cosine, Hamming, sinc, and 10% truncated Gaussian) produced more desirable results than a rectangular weighted scheme [4].

More recently, Guenther and Walker developed apodization functions using a constrained least squares implementation [5], [6]. In that work, apodization functions were created that reduced sidelobe levels below that of a Hamming apodization while maintaining mainlobe width. In another more recent approach, Seo and Yen applied a dual apodization with cross-correlation scheme (DAX) to reduce clutter and sidelobe levels [7]. Finally, Sung and Jeong introduced an apodization method that included multiple apodizations of the same data to achieve sidelobe reduction while maintaining mainlobe width similar to rectangular apodization [10]. In their simulation studies they were able to suppress sidelobe levels by 9 dB while maintaining mainlobe width comparable to rectangular apodization.

The use of apodization has had a long history in shaping radiation patterns in diagnostic ultrasound imaging. Apodization techniques are used to trade mainlobe width for low sidelobes. In this study, a new method of apodization is proposed that will markedly improve the lateral resolution of the imaging system by a factor of five or more times compared to rectangular apodization, while simultaneously keeping sidelobes low. The apodization scheme relies on using a null in the beam pattern to achieve imaging. Because the null of a beam can fall off faster than the roll off of the mainlobe, spatial resolution can be improved over imaging with the mainlobe.

II. Methods

The far-field beam pattern from an ultrasonic transducer or an array is related to the Fourier transform of the product of the aperture function and the apodization function [1]. For

J. Reeg and M. L. Oelze are with the Department of Electrical and Computer Engineering, University of Illinois, Urbana-Champaign IL, 61801 USA e-mail: (oelze@illinois.edu).

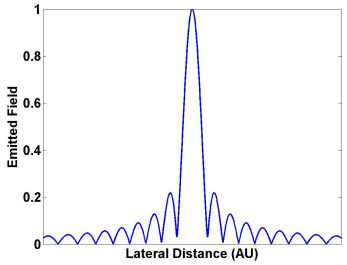

(a)

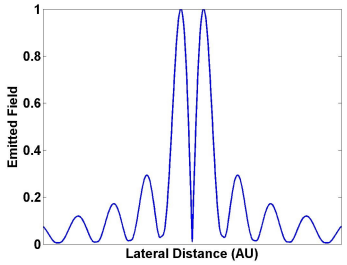

(b)

Fig. 1. Predicted beam patterns of apodization functions. (a) The beam pattern of a transducer where all 32 elements are weighted equally. (b) The beam pattern of the same transducer weighted with a zero mean function.

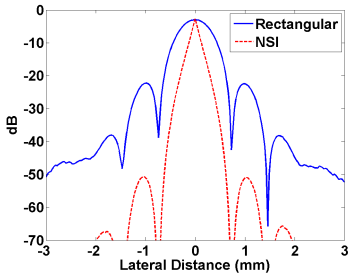

Fig. 2. Illustration of NSI beam pattern vs the rectangular apodization beam pattern.

example, the beam pattern for a rectangular function is a sinc (see Figure 1a). Based on these Fourier transform pairs, the beam pattern from an apodization function with a zero-mean weighting across the array results in a null occurring at broadside. Figure 1b shows a zero-mean apodization function's predicted beam pattern. The beam pattern for a rectangular window (no apodization) maintains a beamwidth limited by diffraction. However, if we compare the width of the rectangular apodization with one minus the zero-mean apodization beam pattern, the shape of the main beam falls off much faster for the 'inverted' null beam. The property of the null beam can be exploited through a novel approach, hereafter referred to as the "bridging" approach, to improve the lateral resolution while maintaining low sidelobes. Figure 2 shows an illustration of the NSI beam pattern with a much narrower beam width.

In the bridging approach, an image is first constructed using the zero-mean apodization. A second image is constructed by taking the zero-mean apodization and adding a small DC constant c to the apodization giving,

$$A_{R,i} = \begin{cases} 1 & : 1 \leq i < \frac{N}{2} \\ -1 & : \frac{N}{2} \leq i \leq N \end{cases} \quad (1)$$

$$A_{R2,i} = A_{R,i} + c. \quad (2)$$

Because using this apodization would put more energy on one side of the beam pattern, a third apodization is constructed by flipping the second apodization. These two new apodized images are beamformed, envelope detected, and added together to produce a new image, i.e., the DC apodization image. This image is nearly equivalent to that of one taken with the null producing apodization, except with a "bridge" of small, positive nonzero values between the two mainlobes of the null beam pattern. The signals acquired using the zero mean apodization are then beamformed, envelope-detected, normalized such that they have the same maximum value, and subtracted from the DC apodization image.

In the DC apodization scheme, an adjustable parameter is the amount of DC bias applied to the apodization weights. By increasing the DC bias, the level of the "bridge" was increased. The level of the DC bias allows a tradeoff between sidelobe levels and mainlobe width. However, above a certain level increasing the DC bias does nothing to improve mainlobe width but still increases sidelobe levels.

III. Experiments

To assess the performance of the novel apodization scheme, experimental measurements were acquired from an ATS539 phantom using an L9-4/38 clinical array transducer (measured center frequency of 5 MHz) and an Ultrasonix RP with a SonixDAQ. A plane wave at broadside was emitted from the transducer array. To reconstruct the images, Delay and Sum (DAS) beamforming was used. The apodizations used in the reconstruction were based off of a zero-mean function where half the elements were weighted at one, and the other half weighted at negative one.

As the results will show, the -6-dB beamwidth was often smaller than the pitch of the array. Therefore, to more accurately characterize the beamwidth of NSI, a finer lateral resolution was required. This was accomplished by acquiring 128 scan lines using plane wave imaging then physically moving the array laterally in steps of 5 microns to fill in additional scan lines. At each position of the array a new set of 128 scan lines was acquired. In total, to span the pitch of the array, the array was moved 61 times with the 5 micron step size.

The ATS539 multi-purpose phantom was used to test the effectiveness of the technique at varying depths, and to evaluate if the technique affected the contrast to noise ratio (CNR) of contrast targets (both hyperechoic and anechoic) in the phantom, with CNR defined by,

$$CNR = \frac{\mu_{in} - \mu_{out}}{[\sigma_{in}^2 - \sigma_{out}^2]^{\frac{1}{2}}}, \quad (3)$$

where μ_{in} is is the mean of the normalized decibel-scale data of the image (E) inside the target, μ_{out} is the mean of (E) outside the target, σ_{in}^2 is the variance of E inside the target,

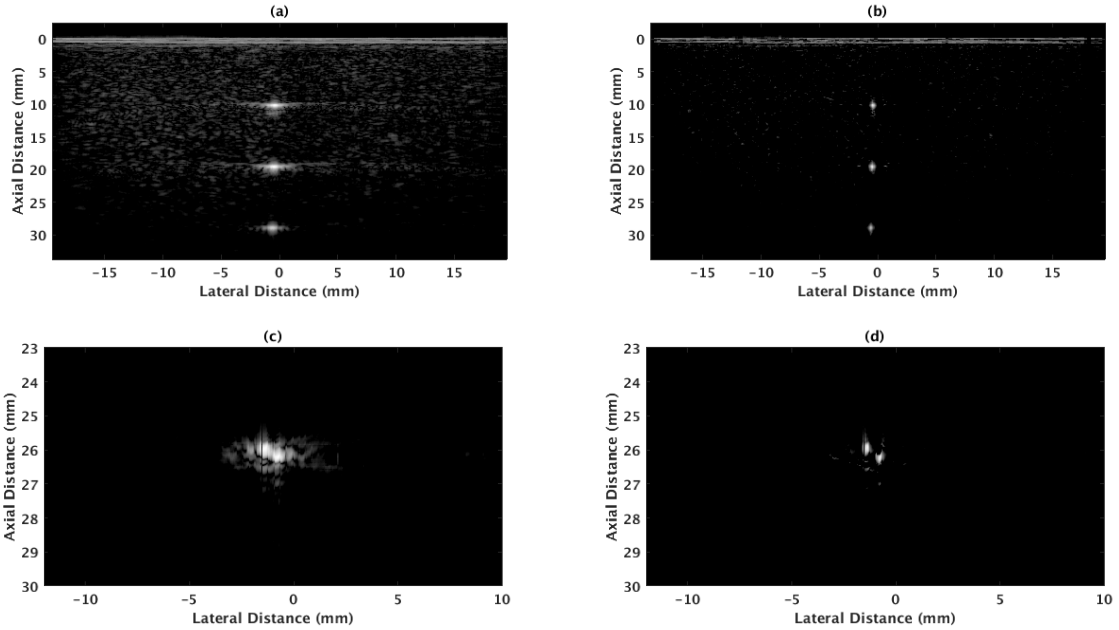

Fig. 3. Images of wire targets. (a) Image of successive targets taken using a rectangular apodization. (b) Image of successive targets taken using NSI. (c) Image of parallel targets spaced $<$ 1 mm apart taken using a rectangular apodization. (d) Image of parallel targets spaced $<$ 1 mm apart taken using NSI.

and σ_{out}^2 is the variance of E outside the target. In addition to the contrast targets, the phantom contained a variety of wire targets in different configurations. These wire targets were made of nylon and had a diameter of 0.12 mm. The L9-4/38 was positioned over the ATS phantom scan window and pulse excited plane waves were emitted at a frequency of 5 MHz and 128 lines of RF data on receive were acquired at a sampling frequency of 40 MHz.

IV. Results

For the wire targets shown in Figures 3a and b, -6 dB beamwidths were recorded for NSI and rectangular apodization at each depth. At successive depths of 1, 2, and 3 cm, the beamwidths for rectangular apodization were 0.64, 0.62, and 0.62 mm respectively. For NSI, they were 0.12, 0.11, and 0.17 mm respectively. Thus an improvement factor of up to 6 times was observed. Since it was verified that NSI improved lateral resolution, images were taken to show that it could also distinguish between two closely placed targets, shown in Figures 3c and d. Sidelobe magnitude also decreased by an average of 17 dB using NSI.

The speckle was also observed to be much finer for NSI images compared to rectangular apodized images. The speckle signal to noise ratio (sSNR), defined by

$$sSNR = \frac{\langle |E| \rangle}{[\langle |E|^2 \rangle - \langle |E| \rangle^2]^{\frac{1}{2}}}, \tag{4}$$

where E is the envelope data of the image, was calculated for the NSI and rectangular apodizations and the results were averaged together. An average sSNR of 1.99 was observed for the rectangular apodization, while an average sSNR of 0.68 was observed for NSI. This indicates that for NSI, the speckle was no longer fully developed.

When examining contrast targets, the CNR was observed to decrease for NSI compared to rectangular apodization. For the hypoechoic targets (Fig. 4a,b,c), a CNR of -0.61 was obtained using NSI, while using a rectangular apodization yielded a CNR of -2.24. To improve the CNR, the rectangular apodized and NSI images were compounded, using 50% of the magnitude of the rectangular image, resulting in a CNR of -1.97. For the hyperechoic targets (Fig. 4d,e,f), a CNR of 0.29 was obtained using NSI, while a CNR of 1.13 was obtained using a rectangular apodization. Once again, the two images were compounded, using 50% of the magnitude of the rectangular image, resulting in a CNR of 0.99. While improvements in CNR were observed, compounding the images also resulted in an increase in the lateral resolution from NSI. These new beamwidths for depths of 1, 2 and 3 cm, were 0.21, 0.20, and 0.28 mm respectively. The CNR metric decreased as the variance of the speckle increased. In the case of the NSI image, the image was more spotty with what appeared to be dark holes in the image and as a result a larger variance of the intensity. On the other hand, the image constructed using rectangular apodization provided a smoother appearance in the contrast target resulting in lower variance in the intensity of the image.

V. Conclusion

With NSI, a factor of improvement in lateral resolution of at up to 6 times compared to the rectangular apodization was achieved experimentally. Improvements in sidelobes by an average of 17 dB over the rectangular apodization were also observed. However, when using NSI the CNR for hyperechoic and anechoic targets were observed to decrease. Compounding NSI with conventional B-mode alleviated some of the loss in CNR. NSI may be useful for identifying small specular targets like microcalcifications in imaging. While the gains in lateral resolution and decreases in sidelobes are dramatic, the

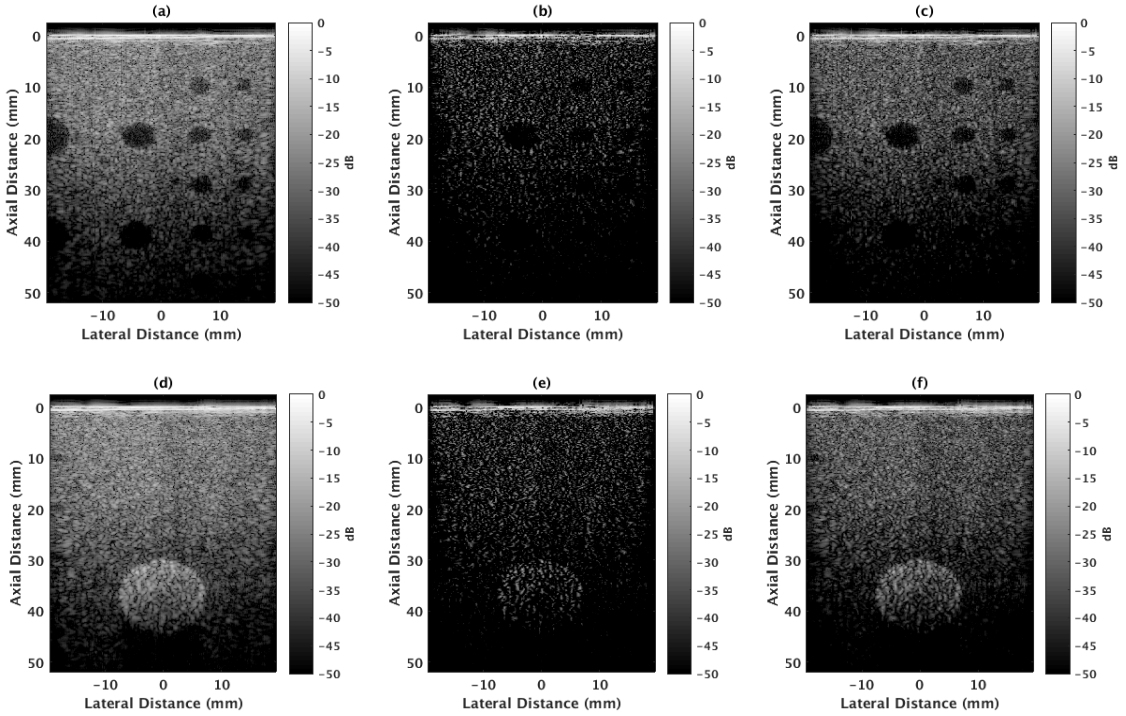

Fig. 4. Images of contrast targets. (a) Hypoechoic targets taken using a rectangular apodization. (b) Hypoechoic targets taken using NSI. (c) Hypoechoic targets, image formed by compounding B-mode (50% weight factor) and NSI. (d) Hyperechoic targets taken using a rectangular apodization. (e) Hyperechoic targets taken using NSI. (f) Hyperechoic targets, image formed by compounding B-mode (50% weight factor) and NSI.

changes to the speckle reduce the ability to see contrast targets. Additional processing is required to alleviate the speckle artifacts produced by the NSI technique, which amounts to trading off some of the gains in lateral resolution for improved contrast.

ACKNOWLEDGMENT

This work was funded by a Strategic Research Initiative Grant from the University of Illinois at Urbana-Champaign.

REFERENCES

[1] F. J. Harris, "On the use of windows for harmonic analysis with the discrete Fourier transform," *Proc. IEEE*, vol. 66, no. 1, pp. 51–83, 1978.

[2] C. L. Dolph, "A Current Distribution for Broadside Arrays Which Optimizes the Relationship between Beam Width and Side-Lobe Level," *Proc. IRE*, vol. 34, no. 6, 1946.

[3] T. T. Taylor, "Design of line-source antennas for narrow beamwidth and low side lobes," *IRE Trans. Antennas Propag.*, vol. 3, no. 1, 1955.

[4] P. J. t'Hoen, "Aperture apodization to reduce the off-axis intensity of the pulsed-mode directivity function of linear arrays," *Ultrasonics*, vol. 20, no. 5, pp. 231–236, 1982.

[5] D. Guenther and W. Walker, "Optimal apodization design for medical ultrasound using constrained least squares part I: theory," *IEEE Trans. Ultrason., Ferroelect., Freq. Control*, vol. 54, no. 2, pp. 332–342, Feb. 2007. [Online]. Available: http://ieeexplore.ieee.org/lpdocs/epic03/wrapper.htm?arnumber=4107692

[6] D. a. Guenther and W. F. Walker, "Optimal apodization design for medical ultrasound using constrained least squares Part II: Simulation results," *IEEE Trans. Ultrason., Ferroelect., Freq. Control*, vol. 54, no. 2, pp. 343–358, 2007.

[7] C. H. Seo and J. T. Yen, "Sidelobe suppression in ultrasound imaging using dual apodization with cross-correlation," *IEEE Trans. Ultrason., Ferroelect., Freq. Control*, vol. 55, no. 10, pp. 2198–2210, 2008.

[8] H. Wang, "System and method for adaptive beamformer apodization," U.S. Patent 6 436 044, Aug. 20, 2002.

[9] J. Guo, L. Chen, Y. Zhang, K. Yang, J. Li, and X. Gao, "Method of ultrasonic phased array imaging based on segment amplitude apodization," 2013, pp. 181–188.

[10] J. Sung and J. Jeong, "Dual-/tri-apodization techniques for high frequency ultrasound imaging: a simulation study," *BioMedical Eng Online*, vol. 13, no. 1, p. 143, 2014. [Online]. Available: http://www.biomedical-engineering-online.com/content/13/1/143

[11] J. A. Jensen, "Field: A program for simulating ultrasound systems," in *Medical & Biological Engineering & Computing*, vol. 34, 1996, pp. 351–353.

[12] J. A. Jensen and N. B. Svendsen, "Calculation of pressure fields from arbitrarily shaped, apodized, and excited ultrasound transducers," *IEEE Trans. Ultrason. Ferroelec. Freq. Control*, vol. 39, pp. 262–267, 1992.

[13] J. Gazdag and S. Piero, "Migration of Seismic Data," *Proc. IEEE*, vol. 72, no. 10, pp. 1302–1315, 1984.

[14] A. S. Savoia, G. Matrone, A. Ramalli, and E. Boni, "Improved Lateral Resolution and Contrast in Ultrasound Imaging Using a Sidelobe Masking Technique," *IEEE International Ultrasonics Symposium*, pp. 1682–1685, 2014.

[15] K. Raum and J. O'Brien, D., "Pulse-echo field distribution measurement technique for high-frequency ultrasound sources," *IEEE International Ultrasonics Symposium*, vol. 2, no. 4, pp. 810–815, 1997.

[16] J. J. Faran, Jr, "Sound scattering by solid cylinders and spheres," *J. Acoust. Soc. Am.*, vol. 23, no. July, pp. 405–418, 1951.